Electrochimica Acta 296 (2019) 1115–1121

Contents lists available at ScienceDirect

Electrochimica Acta

journal homepage: www.elsevier.com/locate/electacta

Electrochemical formation of Cr(III)-based films on Au electrodes

Vera Smulders [a], Nina Simic [b], Adriano S.O. Gomes [b], Bastian Mei [a], Guido Mul [a, *]

[a] PhotoCatalytic Synthesis Group, Faculty of Science and Technology, MESA+ Institute for Nanotechnology, University of Twente, Meander 229, P.O. Box 217, 7500 AE, Enschede, the Netherlands
[b] Nouryon, SE 445-80, Bohus, Sweden

ARTICLE INFO

Article history:
Received 5 October 2018
Received in revised form
7 November 2018
Accepted 9 November 2018
Available online 17 November 2018

Keywords:
Chlorate
Cathode selectivity
Cr(III) oxide film formation
Electrochemical quartz crystal microbalance (eQCM)
Rotating ring disk electrode (RRDE)
Industrial electrochemistry

ABSTRACT

In electrochemical production of sodium chlorate from brine solutions, an intriguing function of sodium (di)chromate is to inhibit cathodic reduction of oxychlorides, while maintaining effective reduction of water to form hydrogen. Using an electrochemical Quartz Crystal Microbalance (eQCM) and a Rotating Ring Disk Electrode (RRDE; Au disk, Pt ring), we analyzed the deposition of reduced Cr-species formed from reduction of $Cr^{VI}O_4^{2-}$ on Au electrodes. Generally, the current induced by reduction of $Cr^{VI}O_4^{2-}$ is significantly larger than the accumulated amount of weight deposited on the Au electrode. Deconvolution of the reductive peak reveals two processes that can be differentiated by varying rotation speed. We therefore propose soluble $Cr^{V}O_4^{3-}$ is formed by reduction of $Cr^{VI}O_4^{2-}$, followed by consecutive reduction of $Cr^{V}O_4^{3-}$ to primarily soluble $Cr^{III}(OH)_4^-$. Simultaneously, reduction of $Cr^{V}O_4^{3-}$ also leads to the formation of a monolayer of Cr^{III}(hydr)oxide. This monolayer significantly inhibits the further reduction of $Cr^{VI}O_4^{2-}$, but allows the film to reach a maximum thickness of approximately 1.85 nm by reduction of surface adsorbed $Cr^{V}O_4^{3-}$ and/or de-hydroxylation of $Cr^{III}(OH)_4^-$. The observation that limitation of film growth is due to film-induced inhibition of reduction of $Cr^{VI}O_4^{2-}$, and significant solubility of $Cr^{III}(OH)_3$ in the form of $Cr^{III}(OH)_4^-$, will aid in the search of a non-toxic chrome-free alternative for inhibition of cathodic reduction of oxychlorides and selective hydrogen evolution in the chlorate process.

1. Introduction

Approximately 3,6 million tons of chlorate are produced annually, of which 3,2 million tons are used in environmentally friendly Elemental Chlorine Free (ECF) bleaching of pulp. The electrochemical production of chlorate requires 20 TWh annually, making it the third-largest electrochemical process by energy consumption [1]. Chlorate is formed in an undivided electrochemical cell by oxidation of brine forming Cl_2 (eq. (1)) followed by solution-based processes (eqs. (3)–(5)), according to the following reactions:

$$2Cl^- \rightarrow Cl_2 + 2e^- \text{(anodic reaction)} \quad (1)$$

$$2H_2O + 2e^- \rightarrow H_2 + 2OH^- \text{(cathodic reaction)} \quad (2)$$

$$Cl_2 + H_2O \rightarrow HClO + Cl^- + H^+ \text{(electrolyte)} \quad (3)$$

$$HClO \leftrightarrow ClO^- + H^+ \text{(electrolyte)} \quad (4)$$

$$2HClO + ClO^- \rightarrow ClO_3^- + 2Cl^- + 2H^+ \text{(bulk electrolyte)} \quad (5)$$

Reduction of oxychlorides is thermodynamically favored over water reduction on e.g. mild steel cathodes used industrially [2]. To prevent reduction of both intermediates (ClO^- and HClO) and product ClO_3^-, sodium chromate ($Na_2Cr_2O_7$) is added to the electrolyte. The chromate Cr(VI) forms a thin film of Cr(III)(hydr)oxide (denoted from here on out as $Cr^{III}O_x$) on the cathode during operation [3], eliminating unwanted reactions and providing selectivity towards the hydrogen evolution reaction (HER) [4–7]. Similarly, in photocatalytic overall water splitting, catalysts consisting of Cr(VI)-derived oxides inhibit the electrochemical oxygen reduction reaction [8–12], while allowing hydrogen evolution with high stability [13,14]. Unfortunately, in both the electrochemical and photocatalytic cases, $Cr^{III}O_x$ is deposited from the highly carcinogenic, six-valence state of Chromium (Cr(VI)), which falls under REACH legislation and is listed in Annex XIV. This means that authorization

* Corresponding author. PhotoCatalytic Synthesis Group, Faculty of Science and Technology, MESA+ Institute for Nanotechnology, University of Twente, Meander 229, P.O. Box 217, 7500 AE, Enschede, the Netherlands.
E-mail address: g.mul@utwente.nl (G. Mul).

https://doi.org/10.1016/j.electacta.2018.11.057
0013-4686/

is needed for usage within the EU *per* September 2017 [15]. For chlorate production, an alternative must be found urgently, so the process can remain economically viable within the EU. In the strive to find a replacement, the properties of the $Cr^{III}O_x$ film have been studied extensively. Work has focused on several aspects of the film, including its structure [3,16], thickness [17], mechanism of selectivity [4,5], the effect of the underlying electrode (Pt [4,5,18,19]), and the improved current density induced by the film [20]. Possible alternatives [21–25] have also been reported. We note that, while it is known that chromium reduction produces more charge than the corresponding oxidation, and it has been proposed that an excess of reduced chromium goes into solution as $Cr(OH)_4^-$ [4], this was not demonstrated or quantified. At the same time a direct 3-electron reduction of Cr(VI) to Cr(III) has been proposed, although similar work on the reverse process, oxidation of Cr(III) to Cr(VI), suggests a series of 1-electron steps including formation of Cr(V) and Cr(IV) [26]. In a very recent review all accumulated knowledge is provided [27].

MnO_x-containing films deposited from permanganate solution have shown similar selectivity towards H_2 production [24], which has much less health concerns. Unfortunately, contrary to chromium, MnO_x film growth is not limited to the nm range. Unlimited film growth would cause larger resistances and higher cell potentials, in addition to other practical problems in industry, including short-circuiting or cell clogging [24]. We therefore focus on understanding the origin of the limited growth of a protective film from $Na_2Cr_2O_7$ ($Cr^{VI}O_4^{2-}$) on Au electrodes in highly alkaline environment, designed to simulate the pH of the electrolyte close to the cathode in an industrial chlorate process. By comparing the increase in mass of the chromium-oxide film, determined using an electrochemical quartz crystal microbalance (eQCM), and the electrochemical response on a rotating ring disc electrode (RRDE), we demonstrate that reduction of $Cr^{VI}O_4^{2-}$ leads to a variety of soluble species, explaining the mismatch between oxidative and reductive charges. We propose a novel mechanism for deposition and growth termination of protective chromium films, which might contribute to the ongoing search for Cr(VI) replacements.

2. Experimental

Experiments were performed at room temperature in a de-aerated Milli-Q water solution (18,2 Ω Millipore) of 0–40 mM $Na_2Cr_2O_7$ (Sigma Aldrich, >99,8%) at pH 13,8, adjusted using NaOH (Sigma Aldrich, >99%) and a Hanna Edge pH meter with HI11310 electrode. The potentiostat used was a BioLogic VSP. The applied counter electrode (CE, anode) consisted of Pt; the Ag/AgCl reference electrode (RE) (with $E^0(Ag/AgCl) = 0,1976\ V\ vs\ SHE$) was home-made using 3 M NaCl (Sigma Aldrich, >99,8%) and Ag wire (Alfa Aesar, >99,98%). Rotating ring disc experiments were performed using a Metrohm Autolab RRDE using a Au disk as working electrode (WE) with a Pt ring. eQCM experiments were performed using a Gamry eQCM 10 M at 5 MHz, and Au-coated crystals from Gamry.

Electrodes and cell were cleaned by thoroughly rinsing with 10% sulfuric acid, then 10% nitric acid, and finally Milli-Q water. Electrodes were additionally cleaned electrochemically in a 10 mM NaOH cleaning solution by cycling 10 times from 0 to 0,75 V vs RHE at 100 mV s^{-1}, before immersion into the Cr-containing electrolyte.

The collection efficiency of the Pt ring electrode was determined using $K_4Fe(CN)_6$ (Sigma Aldrich, >99,95%) and KNO_3 (Sigma Aldrich, >99,99%). The calibration data are summarized in the supporting information (Fig. S1).

The Sauerbrey equation (eq. (6)) [28] was used to determine the difference in mass (Δm) from the shift in resonance frequency f_s of the electrode. This assumes a dense, rigid film, as can be expected for the small Δm found in this work [28].

$$\triangle fs = -\frac{2f_0^2 mn}{\left(\mu_q \rho_q\right)^{\frac{1}{2}}} \tag{6}$$

In this equation, f_s is the resonance frequency, f_0 is the fundamental frequency of the crystal, m is the mass added, n is the harmonic number (i.e. 1), μ_q is the shear modulus (a ratio of sheer stress to shear strain) and ρ_q is the density. The constants in this equation can be summarized into the calibration constant $C_f = 56{,}6\ Hz\ cm^2\ g^{-1}$, giving by eq. (7):

$$\triangle f = -C_f m \tag{7}$$

All voltages are reported versus RHE, calculated using the relation expressed in eq. (8):

$$E_{RHE} = E(Ag/AgCl) + 0,059\ pH + E^0(Ag/AgCl) \tag{8}$$

3. Results and discussion

3.1. Mass vs charge determined by eQCM

Initially, eQCM measurements were used to determine the quantity of $Cr^{III}O_x$ deposited on the Au electrode during electrochemical reduction of dichromate. The potential was cycled from −0,5 to 1,8 V vs. RHE, starting from 0,75 V (close to open circuit potential). The weight changes and the current response observed were measured: a representative experiment in the presence of $Cr^{VI}O_4^{2-}$ is shown in Fig. 1 and the result of a reference experiment in the absence of $Cr^{VI}O_4^{2-}$ is provided in Fig. S2, respectively.

In the absence of $Cr^{VI}O_4^{2-}$ (Fig. S2) the expected currents due to hydrogen (<−0,5 V vs. RHE) and oxygen evolution (>1,5 V vs. RHE) on the Au working electrode were observed, as well as peaks related to the formation (Peak IIa and d) and reduction (peak III) of surface Au_2O_3 [26]. Accordingly, only a small, reversible mass difference of 0,2 μg cm^{-2} was detected at +1,0 to 1,5 V (peak III). When $Cr^{VI}O_4^{2-}$ is added (Fig. 1), a much larger but equally reversible mass difference appears (see Fig. S3 for reproducibility). Mass gain, which takes place only during the cathodic sweep, is initiated simultaneously with $Cr^{VI}O_4^{2-}$ reduction (Peak I), and continues at slower growth rate at more negative potentials (0,17 to −0,5 V). At these potentials a small, but not so obvious current is generated due to the continued reduction of $Cr^{VI}O_4^{2-}$ or intermediates. Similarly, mass loss during the anodic sweep corresponds to the oxidation of the solid deposit to soluble species (Peak IIa and IIc, 1,0 V–1,5 V vs. RHE), as observed in the accompanying CV. Usually, the formation of the solid-deposit on the surface of the electrode is only discussed on the basis of the large reduction peak [3,5], however, as suggested by the eQCM results, film growth continues beyond this potential. Chrono-amperometric measurements (at −0,5 V vs. RHE) revealed that the total mass deposited after 20 min levels off at 0,58 μg cm^{-2}, in good agreement with the calculated mass gain on the basis of measured currents in cyclic voltammetry. The composition of an electrochemically deposited film has been previously proposed, with suggestions being (hydrated) $Cr(OH)_3$ [3], Cr_2O_3 [29], or a mixture of the two [18,19]. Assuming the film is composed of $Cr(OH)_3$, a mass of 0,58 μg cm^{-2} would require 1,6 mC cm^{-2} to reduce sufficient Cr^{VI} to Cr^{III} (Table 1, Q_{eQCM}). Using a density of 3,11 g cm^{-3} for $Cr(OH)_3$, the film can be estimated to be 1,85 nm thick. This can be estimated to be 1 to 3 monolayers, depending on

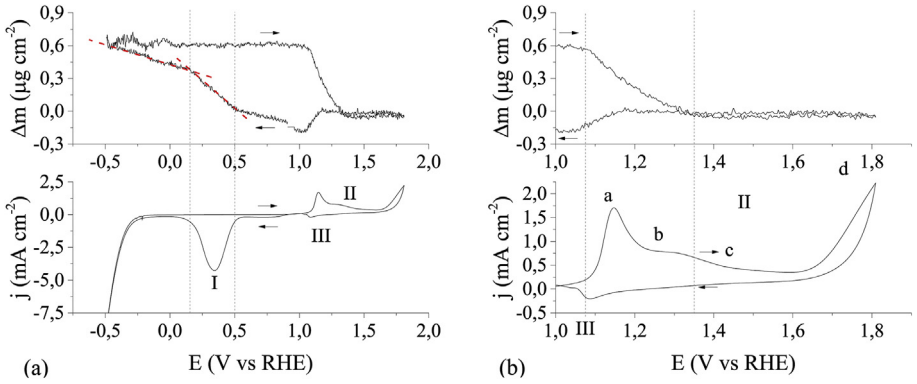

Fig. 1. (a) Cyclic voltammogram (on Au, at 50 mV s^{-1}) and corresponding Δm vs E in 10 mM $Na_2Cr_2O_7$ at pH 13,8. (b) Shows the oxidative range in more detail. Dashed grey lines are a guide to show the onset of mass change. The dashed red lines indicate linear mass change rates. (For interpretation of the references to colour in this figure legend, the reader is referred to the Web version of this article.)

Table 1
Charges corresponding to redox processes. Values displayed in italics should correspond to the Cr(III)-(hydr)oxide film growth.

Source	Charge (mC/cm^2)
Q_{eQCM}: Charge needed for mass gain found in QCM, for Cr(VI) to $Cr(OH)_3$	*−1,6*
$Q_{disc\ ox}$: disc oxidation minus Au oxidation +0,75 V through +1,6 V	*−1,7*
$Q_{disc\ red}$: total disc reduction +0,6 V through −0,1 V	*−45,9*
Q_{ring}: ring oxidation, after efficiency correction, +0,6 V through −0,1 V	*+43,4*
$Q_{RRDE\ net}$: $Q_{disc\ red} - Q_{ring}$	*−2,5*

the method used: assuming the Cr_2O_3 unit cell, it is 1–2 monolayers, but from ellipsometry [17] it would be 2–3 monolayers. This thickness is smaller than found in literature, where it is estimated by XPS to be in the order of 8 nm [3] and by ellipsometry to be 2–4 nm [17]. However, since the $Cr^{III}O_x$ film is likely not composed of stoichiometric $Cr(OH)_3$ but rather similar to a gel-like layer including OH^- and H_2O moieties [3,27], the discrepancy in reported thickness might be explained. Hydration of $Cr(OH)_3$ will add significant volume without causing dramatic changes in film weight. In addition, the finding that 1–3 monolayers of chromium are involved is consistent with previous studies [4,5,18,25]. It should also be mentioned that the mass gain appears to be independent of the concentration of sodium dichromate for concentrations between 10 and 40 mM (see Fig. S4). This result deviates from previous studies, which have shown a dependence of film mass on concentration (in a large concentration range, 0,15 - 15 mM) as well as potential range (−0,6 to −1,7 V vs SCE) [3,17]. Applied experimental conditions and differences in analytical methodology might explain the observed differences.

From the eQCM response it is obvious that there is a clear difference in rate between film formation (marked in Fig. 1a by dashed red lines) and dissolution (region II): the mass gain region during the cathodic sweep contains two clearly distinct linear deposition rates suggesting a two-step process, whereas the mass loss by oxidation of the chromium oxide film happens in a single, rapid step.

Because there are two distinct and linear regions of mass increase, it seems unlikely that the film is self-limiting simply due to its own increased resistance, or that the decrease in deposition rate is due to depletion of Cr(VI) near the electrode; one would expect the mass change to taper off gradually in those scenarios. Instead the distinct change in mass increase observed at approximately 0,38 μg cm^{-2} suggests that there is an abrupt transition in the deposition mechanism. Assuming reduction of $Cr^{VI}O_4^{2-}$ to $Cr(OH)_3$, the mass (0,38 μg cm^{-2}) appears to be sufficient for a complete monolayer coverage. Since no major changes in the electrolyte or in the Au surface appear during deposition, it seems likely that complete coverage of the Au surface by $Cr^{III}O_x$ is the trigger for the decreased deposition rate, before eventually, at 0,58 μg cm^{-2}, the film growth is terminated. This is also indicated by the identical mass change found for different scan speeds, over a range of 5–100 mV s^{-1} (Fig. S5), suggesting film thickness is primarily potential-dependent.

3.2. Characterization of the system using the RRDE

As analysis of the eQCM data shows that reductive current is significantly larger than the oxidative current (Fig. 1a), a Rotating Ring Disc Electrode (RRDE) was used to further analyze the reduction of $Cr^{VI}O_4^{2-}$.

Fig. 2a shows a typical cyclic voltammogram (CV) of a gold electrode (Au disk/Pt ring RRDE) in 10 mM $Na_2Cr_2O_7$ at pH 13,8 at room temperature. $E_{Au,disc}$ is scanned between −0,5 and + 2,25 V vs RHE, starting again from close to the open circuit potential at +0,75 V. The electrode rotation rate was maintained at 4000 rpm, thereby preventing mass transfer limitations, which are inevitable in the eQCM setup and explaining discrepancies in voltammograms between Figs. 1 and 2.

For experiments at high rotation speed (Fig. 2) the Pt ring electrode, E_{ring}, was kept at a constant oxidative potential of +1,5 V vs RHE. The measured ring current was approximately 0 mA in the absence of $Na_2Cr_2O_7$ during the entire sweep (not shown). In the presence of $Na_2Cr_2O_7$ a strong oxidative current, represented by the dashed blue line in Fig. 2a, was detected matching the reductive current associated with the reduction of $Cr^{VI}O_4^{2-}$ observed on the disk. This result - the observation of an oxidative current on the ring - is strong evidence that besides the formation of a $Cr^{III}O_x$ film, soluble, reduced CrO_x-species are formed.

The most pronounced difference when comparing RRDE and eQCM measurements is observed in the oxidative region: as shown in Fig. 1, for the eQCM significantly higher current is obtained in an oxidative scan, as compared to an electrode rotating at 4000 rpm. In the absence of rotation (Fig. S6, solid red), the features of the CV of the disk appear very similar to the data obtained with the eQCM. Holding the disk at the potential of +0,6 V vs RHE for 30 min (without rotation, Fig. S6, dashed red), reduces the intensity of oxidative current in a scan continued in the positive direction, matching the intensities observed at 4000 rpm. This suggests that

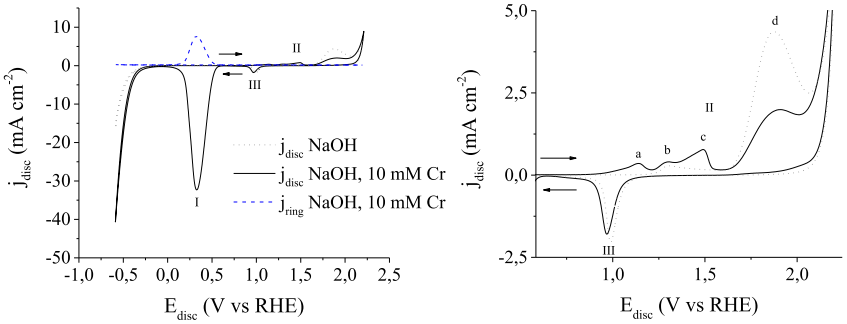

Fig. 2. Cyclic voltammogram at 4000 rpm and 100 mV s^{-1}, RRDE with Au disc working electrode and Pt ring, Ering +1,5 V vs RHE, without (dotted black line) and with 10 mM $Na_2Cr_2O_7$ (solid black line) at pH 13,8. The dashed blue line shows the current on the Pt ring electrode, during the Cr-containing experiment. (a) shows peaks labeled with letters to aid in discussion. (b) Shows the oxidative region of (a) in more detail. (For interpretation of the references to colour in this figure legend, the reader is referred to the Web version of this article.)

aqueous reduced CrO_x-species, formed during the scan in the negative direction, are still in close proximity to the electrode surface, and can be easily re-oxidized in the return sweep. Providing time, or increasing mass transport away from the electrode using rotation, allows to exclusively detect oxidation of the reduced CrO_x film.

The RRDE experiment confirms that reduction and oxidation of $Cr^{VI}O_4^{2-}$ occurs in several steps. In Fig. 2, the negatively-going scan shows a large reduction peak at around +0,4 V (peak I). Because we exclude substantial mass transport limitations at 4000 rpm, we can attribute the decrease in reductive current at potentials more negative than +0.4 V (forming a peak, as opposed to a plateau for a continuous process), purely to inhibition of reduction of $Cr^{VI}O_4^{2-}$ by the *in situ* formed $Cr^{III}O_x$ film, in perfect agreement to the results previously discussed by Lindbergh and Simonsson [5,18].

Detailed analysis of the charges involved in each of the peaks was performed (for detailed information see SI and Fig. S7). The obtained charges are summarized in Table 1, which also includes the charges calculated from the mass gain during the eQCM experiment. The $Q_{eQCM} = 1{,}6\ mC\ cm^{-2}$, mentioned above, is in good agreement with the oxidation of Cr(III) $Q_{disc\ ox} = 1{,}7\ mC\ cm^{-2}$, but much smaller than the charge associated with reduction of Cr(VI) $Q_{disc\ red} = -45{,}9\ mC\ cm^{-2}$. From our eQCM experiments, we assume that $Q_{disc\ ox}$ corresponds to the complete stripping of the $Cr^{III}O_x$ film, also in agreement with recent reports [5]. The reductive charge not accounted for by $Q_{disc\ ox}$ is associated with the current detected at the ring electrode: the corrected ring charge $Q_{ring} = 43{,}4\ mC\ cm^{-2}$. Since solid products cannot be detected at the ring, this charge can be attributed solely to the formation of soluble products. Subtracting Q_{ring} from $Q_{disc\ red}$ leaves a net difference $Q_{RRDE\ net} = -2{,}5\ mC\ cm^{-2}$, which is of the same order of magnitude as Q_{eQCM} and $Q_{disc,ox}$. This clearly demonstrates that the majority of the reductive current is used to produce soluble CrO_x species, and only a small fraction can be attributed to film formation.

Although it is not so obvious in Figs. 1 and 2, the chromium reduction peak is likely the result of multiple reductive processes. This is confirmed by varying the rotation speed of the electrode. The shape of the reduction peak is asymmetrical at low rotation speeds (see Fig. S8). Deconvolution of the peak obtained at 100 rpm, using a semi-quantitative fit, is shown in Fig. 3a.

The plateau current of a mass-transport limited reaction should be linearly dependent on the square root of the angular rotation velocity according to the Levich equation [30]. As previously discussed, there is no mass transport limited current plateau, since an oxide-film is formed at the electrode. Nevertheless, the peak current for the two deconvoluted peaks in Fig. 3a has been used to construct the graph shown in Fig. 3b. Peak Ia shows a linear decrease with rotation rate, suggesting that a mass transfer limited reaction takes place, *prior* to film growth. Peak Ib seems independent of, or even inversely correlated to rotation rate. Independence would suggest the reaction is kinetically controlled, whereas an inverse correlation suggests there is an aqueous intermediate involved in the second reductive process: increased mass transport by higher rotation rates causes this intermediate to be moved away from the electrode surface effectively before it can react further, decreasing the rate and associated current of the consecutive electrochemical reaction [30].

Given the different apparent mass transfer dependences, the ring current was also analyzed in further depth. Fig. 4a shows a

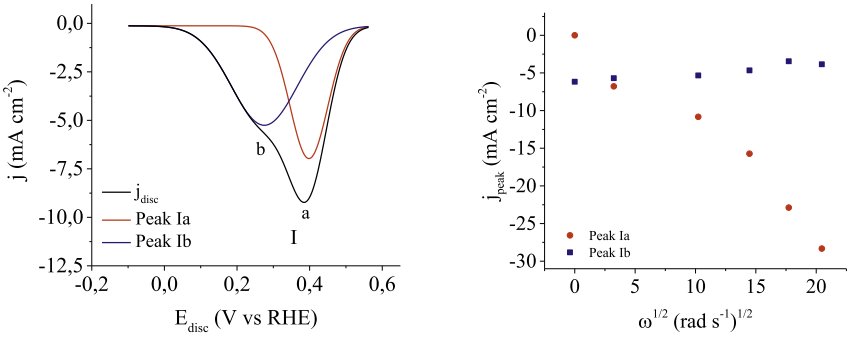

Fig. 3. a) Deconvolution of the reduction peak, CV at 100 rpm, 100 mV s^{-1}; b) area of fitted peaks vs rotation speed. For duplicate measurement see Fig. S9.

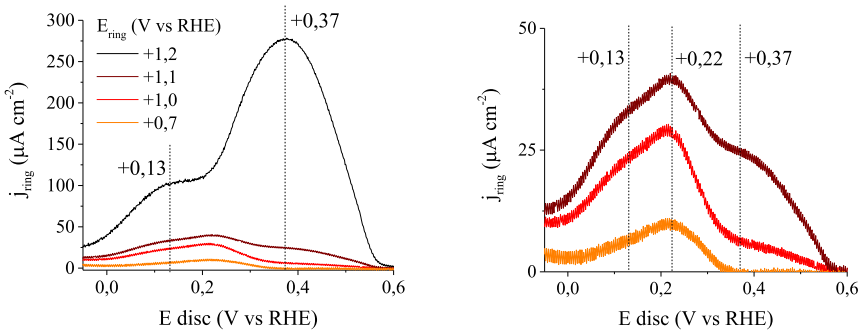

Fig. 4. (a) Ring current versus disc potential, for decreasing ring potentials, during disc cathodic sweep with 10 mM $Na_2Cr_2O_7$, pH 13,8, 4000 rpm and 200 mV s^{-1}, RRDE with Au disc working electrode and Pt ring (as in Fig. 2); b) detail of a).

more detailed view of the ring current as a function of disk potential. Several peaks are observed. Their positions and relative intensities vary based on the applied ring potential. It is difficult to identify the number and origin of the oxidation reactions occurring on the ring with certainty, but at the two most oxidative ring potentials used (+1,5 V and +1,2 V vs RHE), the peak-shape of the oxidation current on the ring is similar to that of the reduction current on the disc (which is much more asymmetrical at the 200 mV s^{-1} used in Fig. 4). The ring peaks are centered at E_{disc} +0,37 V and +0,13 V vs. RHE. This is slightly shifted compared to the reduction peaks of Cr(VI) detected on the disc (+0,33 and + 0,27 V vs. RHE); this may be partly attributed to the time delay it takes for the species to move from the disc to the ring, and partly to kinetic effects, either due to different kinetics for oxidation versus reduction, or because the disc is Au while the ring is Pt.

At less positive ring potentials, $E_{Pt,ring} < +1,2$ V, significantly smaller currents are obtained, as shown in Fig. 4b. Interestingly, the oxidation process belonging to the detected current that peaks at E_{disc} +0,37 V almost disappears, suggesting that E_{ring} +1,2 V is the minimum potential required for the oxidation of this particular species. For even lower applied potentials an oxidative current can still be detected at the ring and it seems as though as many as three peaks may be present. However, only two distinct oxidative reactions dominate, whose peak-overlap results in a variety of peak shapes. At the lowest ring potential used, $E_{Pt,ring} = +0,7$ V, only a single peak is visible at +0,22 V vs RHE, a good match for peak Ia. The various peak shapes can then be explained by a narrow peak at +0,22 V overlapping with a broad peak, that for sufficiently high potentials dominates the +0,37 V region. It is interesting to note that the lowest investigated ring potential, +0,7 V, is well below the onset potential of chromium oxidation on Pt, and in fact only barely more oxidative than required for reduction of Cr(VI) (see Fig. S10). This is in contrast to Au electrodes, where the oxidation of the soluble species occurs in the same potential region, as film oxidation (see also Fig. S6). Fig. S10 also shows that any Pt contamination from the CE [31] should result in a visibly different $Cr^{III}O_x$ formation-mechanism. Since all measurements are consistent with the behavior of Au, Pt contamination of the disk can be safely assumed to be absent.

Thermodynamic data relating to Cr-electrolyte systems can be summarized in a Pourbaix diagram (see Fig. S11, adapted from Ref. [32]). A slight mismatch between actual values of the experiments and the Pourbaix diagram is not surprising, since kinetics, electrode overpotentials, or the iR drop of the cell have not been taken into consideration in constructing the Pourbaix diagram. Experiments were performed at pH 13,8, where thermodynamics suggest chromium exists as chromate, $Cr^{VI}O_4^{2-}$. As a negative potential is applied, $Cr^{VI}O_4^{2-}$ is reduced in a fast, mass transfer limited 1-electron reaction to soluble $Cr^{V}O_4^{3-}$ [26,32], explaining the rotation rate dependence of peak Ia (Fig. 3 and Fig. S8), and the accompanying signal on the ring induced by re-oxidation of $Cr^{V}O_4^{3-}$ to $Cr^{VI}O_4^{2-}$. A consecutive, kinetically limited reduction of $Cr^{V}O_4^{3-}$ leads to formation of lower valence CrO_x species, most likely $Cr^{III}(OH)_4^-$ [4,32]. This is again a soluble species that can be detected on the ring. In addition, solid $Cr^{III}O_x$ is deposited, explaining film formation observed by eQCM [32]. Once a monolayer of $Cr^{III}O_x$ is formed, the reduction of $Cr^{VI}O_4^{2-}$ to $Cr^{V}O_4^{3-}$ is inhibited (similar to inhibition of oxychloride reduction) and the remaining current, quickly decreasing in quantity, is due to the kinetically limited reduction of (surface adsorbed) $Cr^{V}O_4^{3-}$ to some additional $Cr^{III}O_x$. This theory is also supported by work on the oxidation of Cr(III) to Cr(VI), where a three-step mechanism was proposed involving similar intermediates [26].

The slower, but still significant mass gain observed by eQCM in the potential region where almost no reduction currents are recorded (Fig. 1a; $E_{Au} = +0,17$ to $-0,5$ V), suggests previously proposed direct reduction of $Cr^{VI}O_4^{2-}$ to $Cr^{III}O_x$ (s) is improbable [3–5]. We propose an outer-sphere reduction of $Cr^{V}O_4^{3-}$, likely present as surface-bound intermediate, leads to film formation, which is increasingly hampered as the film grows thicker, until the growth is finally terminated entirely. In addition, there could be a direct chemical deposition from the previously formed $Cr^{III}(OH)_4^-$(aq) to $Cr^{III}O_x$(s). However, a small current not present without chromium can be observed in this region (Fig. S2c), corresponding

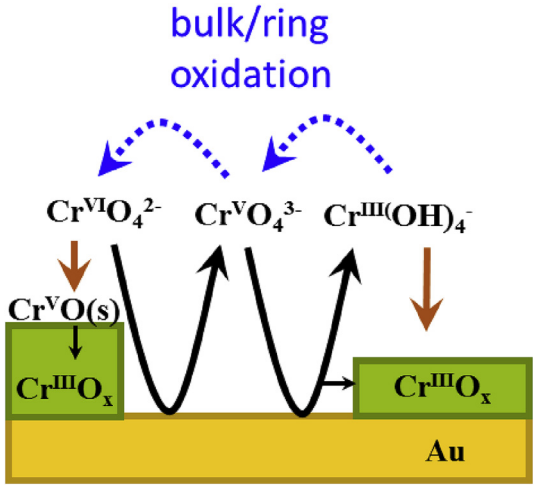

Fig. 5. Schematic overview of the processes occurring on the Au electrode upon reduction of chromate at alkaline pH.

to the current required to deposit the small mass gain (0,05 mA cm^{-2}). QCM measurements at different scan speeds all show the same trend (Fig. S5), indicating a link between film mass and potential, rather than film mass and time. Both these point towards the Faradaic mechanism being dominant, but a chemical deposition cannot be excluded.

In summary, the following electrochemical reduction reactions of $Cr^{VI}O_4^{2-}$ occur on Au electrodes. Please note that the notation above the arrows simply indicates the electrode surface during the reaction, not necessarily the catalytic involvement of this surface.

For the first monolayer E_{Au} = +0,5 to +0,17 V (peak I):

$$Cr^{VI}O_4^{2-}(aq) \overset{Au(s)}{\rightarrow} Cr^{V}O_4^{3-}(aq)$$
(mass transfer limited, rotation dependence of peak Ia) (9)

$$Cr^{V}O_4^{3-}(aq) \overset{Au(s)}{\rightarrow} Cr^{III}(OH)_4^{-}(aq)$$
(kinetically controlled, analysis of peak Ib) (10)

$$Cr^{V}O_4^{3-}(aq) \overset{Au(s)}{\rightarrow} Cr^{III}O_x(S)$$
(kinetically controlled, analysis of peak Ib) (11)

Subsequent layer E_{Au} = +0,17 to −0,5 V where reduction of Cr(VI) is almost entirely suppressed:

$$Cr^{VI}O_4^{2-}(aq) \overset{Cr^{III}O_x(S)}{\longrightarrow} Cr^{V}O_4^{3-}(surface) \quad (12)$$

$$Cr^{V}O_4^{3-}(surface) \overset{Cr^{III}O_x(S)}{\longrightarrow} Cr^{III}O_x(s) \quad (13)$$

The reverse reactions of (9) and (10) probably cause the current detected on the Pt ring of the RRDE, whereas the reverse reaction of (11)–(13) give rise to the oxidative features during film stripping (see Fig. 1, peak II). The mechanism has also been schematically summarized in Fig. 5.

Based on our results, we cannot exclude chemical oxidation of reduced Cr-species by oxychlorides during chlorate production, and this requires further assessment. Nevertheless, our results provide important information about the rich redox chemistry behind the dynamics of chromium film formation and associated self-limiting behavior. For instance, hydroxides of metals less toxic than Cr(VI) (such as Mn(VI) [24]), which form selectivity-inducing films that grow too thickly, could be studied in a similar fashion to determine where their deposition process differs. This could lead to a method with which they could be manipulated to provide limited film growth, so as to enable continued production within the EU by improving the continued production within the EU without using Cr(VI) in the chlorate process.

4. Conclusions

We investigated the dynamics of formation of a film of $Cr^{III}O_x$ from sodium dichromate on Au, using electrochemical and gravimetric methods.

Only a small fraction of reductive charge can be attributed to film growth; the remainder appears to be related to the formation of soluble products. From eQCM data, we find a $Cr^{III}O_x$ film of approximately 1.85 nm in thickness. We propose that reductive deposition of Cr(III) from (di)chromate is preceded by reduction of $Cr^{VI}O_4^{2-}$ to soluble $Cr^{V}O_3^{3-}$, which forms primarily soluble $Cr^{III}(OH)_4^-$ but also a monolayer of $Cr^{III}O_x$. This layer inhibits the further reduction of $Cr^{VI}O_4^{2-}$, similar to the inhibition of reduction of oxychlorides.

Acknowledgments

This research received funding from The Netherlands Organization for Scientific Research (NWO) in the framework of the fund New Chemical Innovations, project 731.015.204 ELECTROGAS, with financial support of Akzo Nobel Chemicals, Shell Global Solutions, Magneto Special Anodes (an Evoqua Brand), and Elson Technologies. Prof. Dr. Detlef Lohse (Physics of Fluids Group, University of Twente, Enschede, The Netherlands) is gratefully acknowledged for valuable discussions.

Appendix A. Supplementary data

Supplementary data to this article can be found online at https://doi.org/10.1016/j.electacta.2018.11.057.

References

[1] R.K.B. Karlsson, A. Cornell, Selectivity between oxygen and chlorine evolution in the chlor-alkali and chlorate processes, Chem. Rev. 116 (2016) 2982.
[2] B. V Tilak, K. Tari, C.L. Hoover, "Metal anodes and hydrogen cathodes: their activity towards O2 evolution and ClO3 – reduction reactions, J. Electrochem. Soc. 135 (1988) 1386.
[3] A. Ahlberg Tidblad, G. Lindbergh, Surface analysis with ESCA and GD-OES of the film formed by cathodic reduction of chromate, Electrochim. Acta 36 (1991) 1605.
[4] G. Lindbergh, D. Simonsson, The effect of chromate addition on cathodic reduction of hypochlorite in hydroxide and chlorate solutions, J. Electrochem. Soc. 137 (1990) 3094.
[5] G. Lindbergh, D. Simonsson, Inhibition of cathode reactions in sodium hydroxide solution containing chromate, Electrochim. Acta 36 (1991) 1985.
[6] C. Wagner, The cathodic reduction of anions and the anodic oxidation of cations, J. Electrochem. Soc. 101 (1954) 181.
[7] W.J. Clark, R.L. McCreery, Inhibition of corrosion-related reduction processes via chromium monolayer formation, J. Electrochem. Soc. 149 (2002) B379.
[8] T. Kanazawa, K. Maeda, Light-induced synthesis of heterojunctioned nanoparticles on a semiconductor as durable cocatalysts for hydrogen evolution, ACS Appl. Mater. Interfaces 8 (2016) 7165.
[9] M. Yoshida, et al., Role and function of noble-metal/Cr-layer core/shell structure cocatalysts for photocatalytic overall water splitting studied by model electrodes, J. Phys. Chem. C 113 (2009) 10151.
[10] K. Maeda, K. Teramura, D. Lu, N. Saito, Y. Inoue, K. Domen, Roles of Rh/Cr2O3 (Core/Shell) nanoparticles photodeposited on visible-light-responsive (Ga1-xZnx)(N1-xOx) solid solutions in photocatalytic overall water splitting, J. Phys. Chem. C 111 (2007) 7554.
[11] K. Maeda, K. Teramura, D. Lu, N. Saito, Y. Inoue, K. Domen, Noble-Metal/Cr2O3 core/shell nanoparticles as a cocatalyst for photocatalytic overall water splitting, Angew. Chem. Int. Ed. 45 (2006) 7806.
[12] M. Qureshi, T. Shinagawa, N. Tsiapis, K. Takanabe, Exclusive hydrogen generation by electrocatalysts coated with an amorphous chromium-based layer achieving efficient overall water splitting, ACS Sustain. Chem. Eng. 5 (2017) 8079.
[13] G.W. Busser, et al., Photodeposition of copper and chromia on gallium oxide: the role of co-catalysts in photocatalytic water splitting, ChemSusChem 7 (2014) 1030.
[14] G.W. Busser, et al., Cocatalyst designing: a regenerable molybdenum-containing ternary cocatalyst system for efficient photocatalytic water splitting, ACS Catal. 5 (2015) 5530.
[15] European Chemicals Agency (ECHA), Authorization list (Annex XIV of REACH). https://echa.europa.eu/addressing-chemicals-of-concern/authorisation/recommendation-for-inclusion-in-the-authorisation-list/authorisation-list, 2015. (Accessed 19 April 2018).
[16] A. Gomes, N. Simic, M. Wildlock, A. Martinelli, E. Ahlberg, Electrochemical investigation of the hydrogen evolution reaction on electrodeposited films of Cr(OH)3 and Cr2O3 in mild alkaline solutions, Electrocatalysis 9 (2017) 333.
[17] A.A. Tidblad, J. Martensson, In situ ellipsometric characterization of films formed by cathodic reduction of chromate, Electrochim. Acta 42 (1997) 389.
[18] A. Cornell, G. Lindbergh, D. Simonsson, The effect of addition of chromate on the hydrogen evolution reaction and on iron oxidation in hydroxide and chlorate solutions, Electrochim. Acta 37 (1992) 1873.
[19] K. Hedenstedt, A.S.O. Gomes, M. Busch, E. Ahlberg, Study of hypochlorite reduction related to the sodium chlorate process, Electrocatalysis 7 (2016) 326.
[20] J. Wulff, A. Cornell, Cathodic current efficiency in the chlorate process, J. Appl. Electrochem. 37 (2006) 181–186.
[21] J. Gustavsson, L. Nylén, A. Cornell, Rare earth metal salts as potential alternatives to Cr(VI) in the chlorate process, J. Appl. Electrochem. 40 (2010) 1529.
[22] L. Nylén, J. Gustavsson, A. Cornell, Cathodic reactions on an iron RDE in the presence of Y(III), J. Electrochem. Soc. 155 (2008) E136.

[23] J. Gustavsson, A. Cornell, G. Lindbergh, J. Bäckström, In-situ Activated Hydrogen Evolution from PH-neutral Electrolyes, KTH Royal Institute of Technology, Sweden, 2012.
[24] B. Endrődi, et al., Towards sustainable chlorate production: the effect of permanganate addition on current efficiency, J. Clean. Prod. 182 (2018) 529.
[25] A.S.O. Gomes, M. Busch, M. Wildlock, N. Simic, E. Ahlberg, Understanding selectivity in the chlorate process: a step towards efficient hydrogen production, ChemistrySelect 3 (2018) 6683.
[26] C.M. Welch, M.E. Hyde, O. Nekrassova, R.G. Compton, The oxidation of trivalent chromium at polycrystalline gold electrodes, Phys. Chem. Chem. Phys. 6 (2004) 3153.
[27] B. Endrődi, N. Simic, M. Wildlock, A. Cornell, A review of chromium(VI) use in chlorate electrolysis: functions, challenges and suggested alternatives, Electrochim. Acta 234 (2017) 108.
[28] J. Kankare, Sauerbrey equation of quartz crystal microbalance in liquid medium, Langmuir 18 (2002) 7092.
[29] J.J. Hatch, A.A. Gewirth, Potential dependent chromate adsorption on gold, J. Electrochem. Soc. 156 (2009) D497.
[30] A.J. Bard, L.R. Faulkner, Electrochemical Methods: Fundamentals and Applications, Wiley, 2000.
[31] J.G. Chen, C.W. Jones, S. Linic, V.R. Stamenkovic, Best practices in pursuit of topics in heterogeneous electrocatalysis, ACS Catal. 7 (2017) 6392.
[32] G.H. Kelsall, C.I. House, F.P. Gudyanga, Chemical and electrochemical equilibria and kinetics in aqueous Cr(III)/Cr(II) Chloride solutions, J. Electroanal. Chem. Interfacial Electrochem. 244 (1988) 179.